Available online at www.sciencedirect.com
ScienceDirect
Aerosol Science 38 (2007) 289–304
Journal of Aerosol Science
www.elsevier.com/locate/jaerosci

The condensation particle counter battery (CPCB): A new tool to investigate the activation properties of nanoparticles

Markku Kulmala[a,*], Genrik Mordas[a], Tuukka Petäjä[a], Tiia Grönholm[a], Pasi P. Aalto[a], Hanna Vehkamäki[a], Anca I. Hienola[a], Erik Herrmann[a], Mikko Sipilä[a], Ilona Riipinen[a], Hanna E. Manninen[a], Kaarle Hämeri[a], Frank Stratmann[a,b], Merete Bilde[c], Paul M. Winkler[d], Wolfram Birmili[a,b], Paul E. Wagner[d]

[a]*Department of Physical Sciences, University of Helsinki, P.O. Box 64, FI-00014 Helsinki, Finland*
[b]*Institute for Tropospheric Research, Permoserstrasse 15, D-04318 Leipzig, Germany*
[c]*University of Copenhagen, Department of Chemistry, Universitetsparken 5, DK-2100 Copenhagen Ø, Denmark*
[d]*Institut für Experimentalphysik, Universität Wien, Boltzmanngasse 5, A-1090 Wien, Austria*

Received 29 June 2006; received in revised form 11 November 2006; accepted 20 November 2006

Abstract

The formation and growth of fresh atmospheric aerosol particles was investigated using a condensation particle counter battery (CPCB). This instrument is a matrix of four separate CPCs, which differ in the combination of both cut-off size and working liquid (water; *n*-butanol). In a first step, the CPC counting efficiencies and cut-off sizes were carefully characterised under laboratory conditions for different condensing vapours, temperature differences between condenser and saturator, and test aerosol types. In addition, the activation process was described theoretically, and modelled numerically for the given CPC configurations. These results confirmed that water-soluble and water-insoluble as well as butanol-soluble and butanol-insoluble aerosol particles may be discriminated in the CPCB through different activation diameters. Therefore, the CPCB represents a novel tool to infer information on the chemical composition of aerosol particles between 2 and 20 nm. To test the applicability of the CPCB under field conditions, the CPCB was operated at a rural background station in Finland (Hyytiälä) in April and May 2005. The results indicate that growing nucleation mode particles were water-soluble both at 3 and 11 nm.

Keywords: CPC battery; Nanoparticles; Chemical composition

1. Introduction

Atmospheric aerosol particles affect the quality of our life in many different ways. In polluted urban environments, atmospheric aerosols may exert adverse effects on human health (e.g., Donaldson, Li, & MacNee, 1998; Stieb, Judek, & Burnett, 2002) and deteriorate visibility (Cabada, Khlystov, Wittig, Pilinis, & Pandis, 2004). In regional and global scales, aerosol particles have a potential to change climate patterns and the hydrological cycle (Lohmann & Feichter, 2005; Ramanathan, Crutzen, Kiehl, & Rosenfeld, 2001; Sekiguchi et al., 2003). A better understanding of the

* Corresponding author.
E-mail address: markku.kulmala@helsinki.fi (M. Kulmala).

0021-8502/$ - see front matter © 2006 Elsevier Ltd. All rights reserved.
doi:10.1016/j.jaerosci.2006.11.008

various effects of atmospheric aerosols requires a more comprehensive knowledge on their sources, and atmospheric transformation and deposition processes. An important phenomenon controlling the number concentration of aerosols in the atmosphere is new particle formation from gaseous precursors, which involves the production of nanometer-size particles by nucleation and their subsequent growth to detectable sizes (Birmili et al., 2003; Kulmala, 2003; Weber et al., 1999). It is now well established from over 100 individual studies that aerosol formation followed by condensational growth up to the 50–200 nm size range may occur in almost any part of the troposphere (Kulmala, Vehkamäki, et al., 2004).

An important gap of knowledge, however, concerns the detailed molecular processes underlying particle nucleation and subsequent growth. A direct determination of the composition of nucleation mode particles (< 20 nm) has usually been hampered by the minuscule amounts of matter available for chemical analysis. Instead, researchers needed to rely on observations using indirect methods, such as particle growth determination in a condensation particle counter (O'Dowd, Aalto, Hameri, Kulmala, & Hoffmann, 2002), and size change analysis through particle humidification (Väkevä, Kulmala, Stratmann, & Hämeri, 2002) or volatilisation (Wehner et al., 2005). Very recently, thermal desorption chemical ionisation mass spectrometry has been demonstrated to yield information on the chemical composition of nanoparticles as small as 6 nm (Smith et al., 2005). New insights into the formation and growth processes of atmospheric nanoparticles, and its relation to particle chemical composition, will depend on the enhancement of these methods, or the development of further techniques to characterise nanoparticles (< 10 nm in diameter) in near real time.

In this paper we introduce a novel application based on the well-established principle of particle detection by vapour activation in a condensation particle counter (CPC). The principle of the CPC consists of three processes: (1) creation of a supersaturated vapour (working fluid); (2) growth of aerosol particles by condensation of these supersaturated vapours; (3) optical detection of the particles after their growth. Different types of CPCs have different techniques of creating vapour supersaturation. The most common type is the laminar flow chamber CPC, which has no movable parts and therefore is suitable for long-term atmospheric observations. Recent developments of CPCs in general have aimed, for instance, at improving the detection efficiency (Stoltzenburg & McMurry, 1991) and response time (Sgro & Fernández de la Mora, 2004). For a comprehensive summary of the history and principles of CPCs see e.g. McMurry (2000).

The detection efficiency of a CPC is the fraction of particles of a given size that will be activated to a large droplet—typically larger than 10 μm in size. The detection efficiency is a function that is ideally unity for large particles, but drops to zero with decreasing particle size as a result of the Kelvin effect and transport losses inside the CPC. The cut-off diameter of a CPC is commonly defined as the particle diameter at which the detection efficiency is 50%. Stoltzenburg and McMurry (1991) showed that the cut-off diameter is above all a function of the activation efficiency. Hence, for a laminar flow CPC based on the conductive cooling principle the cut-off diameter is essentially a function of the temperature difference (ΔT) between saturator and condenser.

There are several widely used commercial alcohol based CPCs (notably the models 3010, 3022, 3025, 3007, TSI Inc., St Paul, MN, U.S.A.) in which the supersaturation of the alcohol vapour is created by conductive cooling (for performance details, see, e.g., Hämeri, Koponen, Aalto, & Kulmala, 2002; Sem, 2002). Different research groups have tested and calibrated these instruments. Recently, a new generation of commercial CPCs was introduced, where supersaturations are achieved by differences in the molecular water vapour diffusivity and the thermal diffusivity of air (models 3785 and 3786, TSI Inc.; see Hering & Stoltzenburg, 2005). This new technique allows using water as a working fluid. In this paper, we will call the TSI-3785 "Water CPC" (WCPC) and the TSI-3786 "Ultrafine Water CPC" (UWCPC). For previous studies on the performance and detection efficiency of these CPCs see Hering, Stoltzenburg, Quant, Oberreit, and Keady (2005), Biswas, Fine, Geller, Hering, and Sioutas (2005) and Petäjä et al. (2006).

In laminar flow butanol or water-based CPC the detection efficiency can be modified by changing the temperature difference between saturator and condenser (or growth tube). Raising the ΔT will increase the saturation ratio and, consequently, decrease the cut-off diameter. In practice, particle size distributions have been measured by changing the ΔT (Brock et al., 2000; Kulmala, Lehtinen, Laakso, Mordas, & Hämeri, 2005). Brock developed the nuclei-mode aerosol size spectrometer utilizing Kelvin-effect sizing to obtain fast-time response (~ 1 s) airborne measurements. Kulmala et al. performed studies using increasing ΔT between saturator and condenser to have different cut-off diameters in order to be able to detect neutral clusters.

As mentioned before, the CPC detection efficiency depends on the activation probability. The activation process depends directly on the physico-chemical properties of the investigated aerosol particles. In the case of soluble particles, the activation process can be described within the framework of Köhler theory (e.g. Kulmala, Kerminen, Anttila,

Laaksonen, & O'Dowd, 2004). The activation of insoluble particles is described by heterogeneous nucleation theory (Lazaridis, Kulmala, & Gorbunov, 1992). The activation probability (or nucleation probability) is commonly used in laboratory studies of heterogeneous nucleation (see e.g. Kulmala, Lauri, et al., 2001; Wagner et al., 2003). The only difference between the nucleation studies and the studies of CPC detection efficiency is that the former measures the activation probability as a function of the saturation ratio, whereas the latter describes the activation probability as a function of particle diameter.

In this paper we first explain the concept of the condensation particle counter battery (CPCB), thereby supplying the corresponding theoretical framework. Next, we report on the detection efficiency of the four CPCs involved (TSI-3785, TSI-3786, TSI-3010, and TSI-3025) as determined through computational fluid dynamics modelling. The predicted effects of the condenser/saturator temperature difference, i.e. the degree of supersaturation obtained inside the instruments, on the particle detection efficiency are then verified experimentally using a variety of test aerosol particles (Ag, $(NH_4)_2SO_4$, NaCl). The differences in the solubilities of these particle types and the resulting variation in activation probabilities inside the counters are evaluated. Finally, we demonstrate the applicability of the CPCB at atmospheric conditions.

2. Materials and methods

2.1. Condensation particle counter battery (CPCB)

Our CPCB is composed of four individual CPCs, which are operated in parallel. Fig. 1 shows the arrangement of the four CPCs, which represent a 2 × 2 matrix of different cut-offs (3 and 11 nm), as well as different working liquids (*n*-butanol and water). As indicated in Fig. 1, the pair of CPCs (TSI-3010, TSI-3785) as well as the pair of UCPCs (TSI-3025, TSI-3786) are designed so that the same count rates are expected for particle materials that show affinity neither to water nor to butanol. Owing to the increased activation probability in water vapour, however, hygroscopic particles will be detected down to lower particle sizes in the water CPCs; therefore an increased count rate will be measured in comparison to the butanol CPCs. The differential signal between the water and butanol CPCs of each pair is then expected to be related to the presence of hygroscopic particles in the size range of the corresponding cut-off regions. For lipophilic particles, i.e., particles that attract non-polar organic compounds and tend to be hydrophobic, the reverse may be true: If the activation probability of lipophilic particles is higher in butanol vapour than in water, the CPCB will be sensitive to the presence of lipophilic particles in the size range of the two cut-offs. In conclusion, our CPCB represents a new concept to determine simultaneously the affinity of both, 3 and 11 nm particles towards water and butanol vapours.

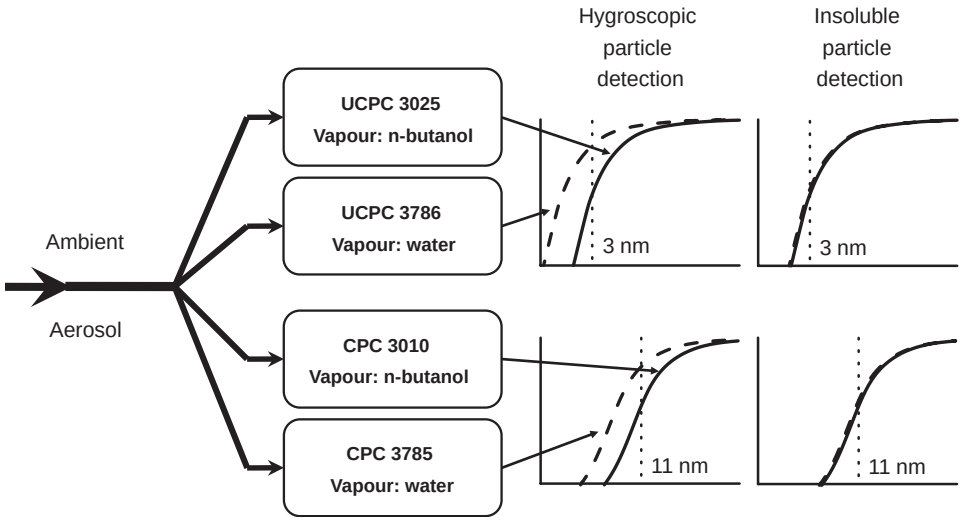

Fig. 1. Principle of the condensation particle counter battery (CPCB).

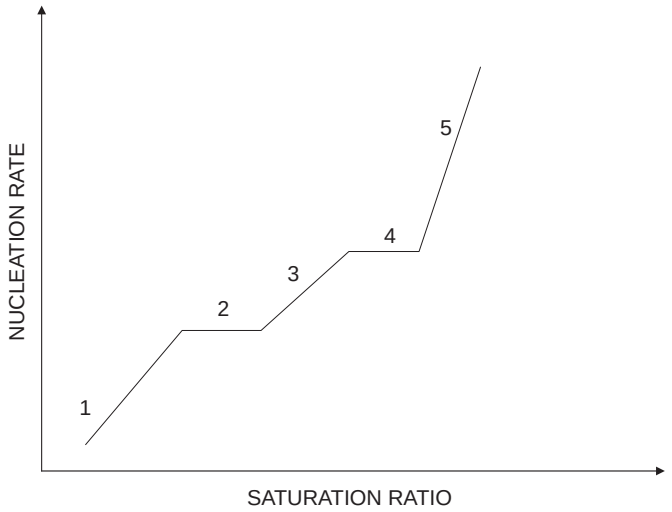

Fig. 2. Particle activation and nucleation inside a CPC as a function of the saturation ratio. In regime 1 ion clusters are activated, in regime 3 neutral clusters, whereas in regime 5 homogeneous nucleation is the dominating process. In regimes 2 and 4 the number of activated particles stays constants.

To determine the "reference state" of the CPCB for insoluble particles, the detection efficiencies of all four CPCs were carefully measured using the calibration set-up described by Petäjä et al. (2006). Briefly, practically monodisperse and spherical silver particles below 40 nm were generated by a combination of a furnace generator and a differential mobility analyser (Scheibel & Porstendörfer, 1983). The cut-off sizes of the two butanol CPCs, the TSI-3025 and the TSI-3010 were determined to be 3 and 11 nm, respectively. The cut-off sizes of the two water CPCs, the TSI-3786 and the TSI-3785 were adjusted so that they matched very closely the cut-off of the corresponding butanol CPCs; in practice this was achieved by varying the saturator/condenser ΔT inside the water CPCs until agreement between the cut-off diameters was reached. The particular temperature differences were 70 K for the TSI 3786, and 25 K for the TSI 3785, and were used as operational values during all subsequent experiments. More details on the temperature settings of the CPCs are discussed below.

2.2. Theoretical background

Besides detecting aerosol particles CPCs can also be used to detect small molecular clusters (e.g., Kulmala et al., 2005). When the saturation ratio is increased above a certain limit by increasing the ΔT in a CPC, ion clusters will be activated first. Further increase of the saturation ratio will then also activate neutrally charged clusters and finally, new particles are formed via homogeneous nucleation. The activation of these particle and cluster types along with increasing supersaturation is illustrated in Fig. 2. As described above, by varying ΔT and the type of condensing vapour we can obtain information on the size and chemical composition of an aerosol population.

In the following, we establish quantitative relationships between the instrumental CPC parameters, notably ΔT and the particle activation probability. Under a given temperature difference, there is a unique spatial profile of saturation ratio inside the CPC condenser tube. Saturation ratio and temperature profiles inside the UWCPC and WCPC were estimated using FLUENT (version 6.2.16, Fluent Inc.) and the Fine Particle Model (FPM, version 1.2.6, particle dynamics GmbH). We simulated the flow tube of the instrument which consists of saturator and condenser. As in the actual UWCPC, the tube has a diameter of 9.5 mm. In the simulation setup, the tube has a length of altogether 30 cm, of which 20 cm are the condenser. The short saturator is sufficient to reach stable, laminar flow conditions. The water vapour content of the air is introduced as a boundary condition at the tube inlet. At a total flow rate of 1 l min^{-1}, the 20 cm of the condenser offer enough length to observe the whole saturation ratio profile. After the simulated condenser, saturation ratio (S) has decreased to about 1, independently of the specific setup. The three-dimensional mesh geometry was created with Gambit (version 2.2.30, Fluent Inc.), and consists of ca. 150 000 cells of about uniform size.

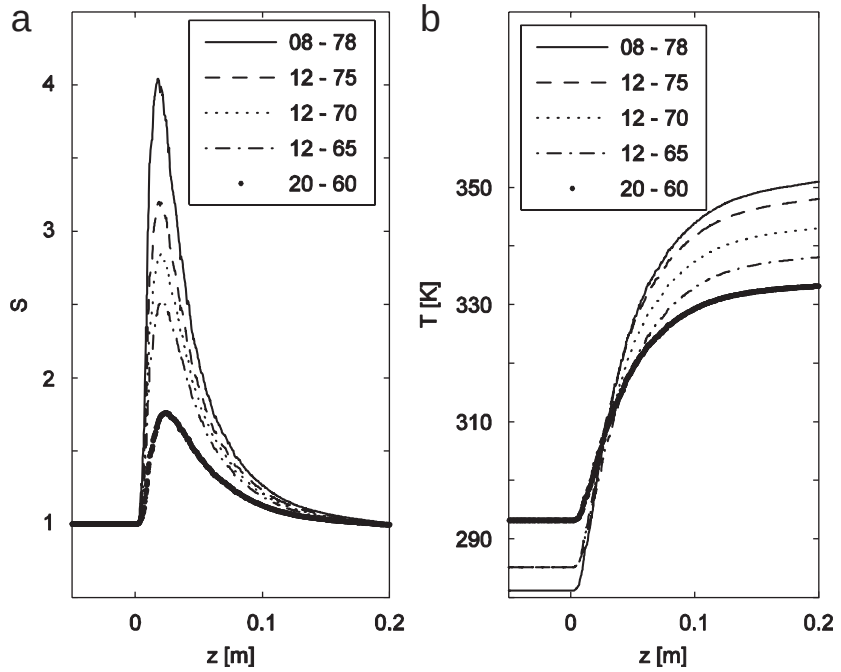

Fig. 3. Profiles of saturation ratio S and temperature T on the centre axis of the flow tube inside the UWCPC obtained from CFD modelling for different saturator (lower temperature) and growth tube (higher temperature) temperature settings. Z is the distance from the starting point of the growth tube.

The key properties in this simulation are the thermal diffusivity of air α_t and the vapour mass diffusivity α_v for water vapour in air. To be able to roughly compare our results to recent ones by Hering et al. (2005) and Hering and Stoltzenburg (2005), those properties were set to be $\alpha_t = 0.215\,\mathrm{cm^2\,s^{-1}}$ and $\alpha_v = 0.265\,\mathrm{cm^2\,s^{-1}}$. However, an exact result match was not possible since the remaining properties were not specified by the authors. In case of uncertainty we used Fluent and FPM standard definitions.

At the entrance of the condenser section, the simulation needs to provide a laminar flow that contains stable amounts of water vapour and temperature. This can be achieved by starting the flow simulation some pathway upstream the condenser, i.e., in the saturator. In our simulation, the sole purpose of the saturator was to provide an entry length for the flow. Temperature and vapour content of the saturated air ($S = 1$) that are supposed to enter the condenser are set as boundary conditions at the inlet to the saturator as well as at its walls. Also the walls of the condenser are set to a slightly higher temperature, and the respective vapour content was initialised to that $S = 1$.

We simulated five different combinations of saturator and condenser temperatures. Fig. 3 shows the resulting saturation ratio and temperature profiles on the central axis of the flow tube. For all setups, S is close to 1 after 20 cm. The temperature at the centre of the tube is close to wall values at the end of the simulated condenser. For all simulations, the maximum of S is located at about 2 cm into the condenser; this value is slightly decreasing with growing saturation ratio. The simulations show also that the saturation ratio is a function of the concentration of aerosol particles, and it decreases as increasing aerosol concentration.

The time evolution of the concentration of dry particles N_{dry} entering the CPC can be solved from equation

$$\frac{\mathrm{d}N_{\mathrm{dry}}}{\mathrm{d}t} = -kN_{\mathrm{dry}} \tag{1}$$

as a result

$$N_{\mathrm{dry}} = N^0_{\mathrm{dry}}\,\exp(-kt)$$

and thus the activation probability P, which is the concentration of activated particles ($N^0_{\mathrm{dry}} - N_{\mathrm{dry}}$) divided by the initial concentration of dry particles, N^0_{dry}, is given by

$$P = \frac{N_{\mathrm{act}}}{N^0_{\mathrm{dry}}} = 1 - \exp(-kt). \tag{2}$$

In the preceding equations k is a proportionality coefficient which is related to either (a) heterogeneous nucleation, or (b) Köhler type activation.

In the case of heterogeneous nucleation

$$k = 4\pi r^2_{\mathrm{dry}} I, \tag{3}$$

where I is heterogeneous nucleation rate per unit area of pre-existing aerosol particle (see e.g. Kulmala, Lauri, et al., 2001).

In the case of Köhler activation k is zero when the radius is smaller than Köhler activation radius (see e.g. Seinfeld & Pandis, 1998) and infinity if radius is bigger than Köhler activation radius.

In the case of soluble (either to water or butanol) particles the saturation ratio needed to activate the aerosol particles is obtained using Köhler theory for small particles (nano-Köhler theory, see Kulmala, Kerminen, et al., 2004). This theory is analogous to the traditional Köhler theory (e.g. Seinfeld & Pandis, 1998) which describes the formation of cloud drops around water soluble aerosol nuclei with the difference that instead of being dry aerosols, the seed particles consist of aerosol–butanol or aerosol–water solution. In a vapour in equilibrium with a droplet having dry radius r_{dry} , the saturation ratio S_i is

$$S_i = x_i \Gamma_i \exp\left(\frac{a_i}{r_{\mathrm{dry}}}\right), \tag{4}$$

where $a_i = 2\sigma v_i / RT$. Here the subscript i denotes butanol or water, x_i is the mole fraction, Γ_i the activity coefficient and v_i is the partial molar volume of component i, σ is the surface tension, R is the molar gas constant and T is the temperature. Eq. (4) gives butanol or water equilibrium curves for different aerosol sizes and compositions. When the saturation ratio inside the CPC is higher than needed for a certain aerosol size according to Eq. (4) , the aerosol particles will activate.

3. Results and discussion

3.1. Theoretical nucleation probability

The CPC detection efficiency depends on the saturation ratio in the condenser tube, and also on composition of aerosol particles and their number concentration. To determine the activation probabilities for different types of aerosol particles we calculated the heterogeneous nucleation probabilities as well as activation probabilities for soluble and insoluble particles. Since homogeneous nucleation has been thought to give the upper limit for the operational saturation ratio inside the CPC we also calculated corresponding Kelvin diameters. The results for water are shown in Fig. 4a and for butanol vapour in Fig. 4b. Heterogeneous nucleation probabilities were calculated for totally wettable particles ($m = 1.0$, i.e., contact angle is zero), and for somewhat hydrophobic particles ($m = 0.5$, i.e., contact angle is 60°). In the case of water vapour, activation probabilities for soluble particles were calculated for sodium chloride (NaCl) and ammonium sulphate ($(NH_4)_2SO_4$) particles. The thermodynamic data for NaCl- and $(NH_4)_2SO_4$–water solutions were obtained from Hämeri, Väkevä, Hansson, and Laaksonen (2001) and Hämeri, Laaksonen, Väkevä, and Suni (2001), respectively. In the case of butanol vapour, thermodynamic data is lacking, so we assumed particles to form an ideal solution with butanol.

As shown in Figs. 4a and b the saturation ratio needed for activation increases when the dry radius of aerosol particle decreases. For soluble and totally wettable particles the activation diameter is smaller than the Kelvin diameter at certain saturation. This important result suggests that homogeneous nucleation will not occur before activation, thus confirming the hypothesis shown in Fig. 2. On the other hand, if one increases the contact angle to examine the effect of the particle surface characteristics on the nucleation probability, the activation diameter becomes larger than the Kelvin diameter.

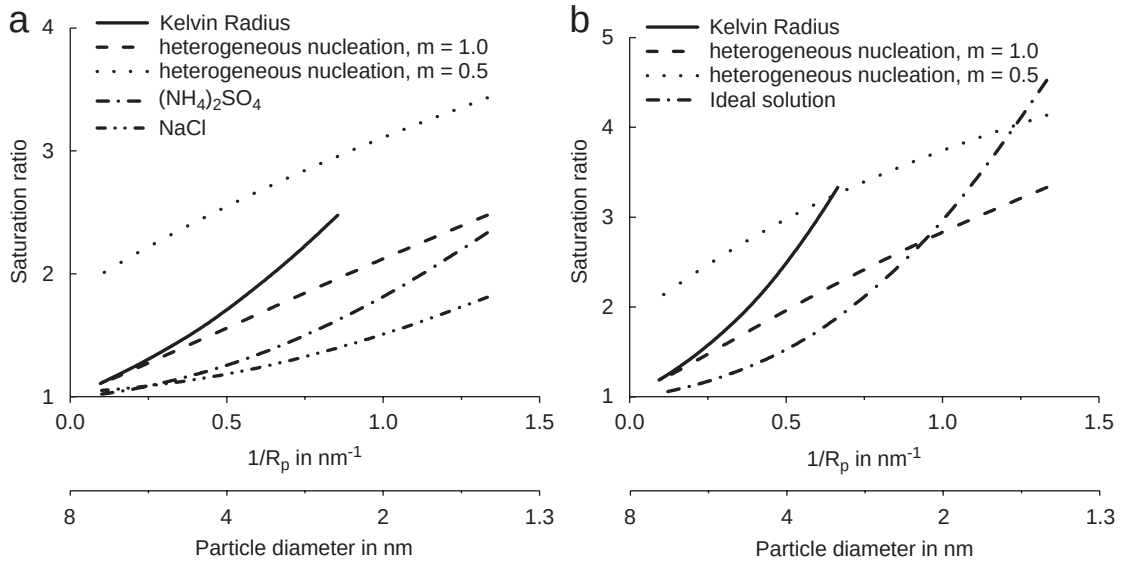

Fig. 4. Saturation ratio as a function of inverse particle radius $1/R_d$ and particle diameter D_p, (a) for water vapour, (b) for butanol vapour.

The effect of solubility is seen by comparing the activation of NaCl and ($(NH_4)_2SO_4$) particles: in the case of water, ammonium sulphate particles seem to activate less effectively than NaCl particles. As seen in the case of the butanol CPCs (see Fig. 4b), the ideal solution particles activate less effectively than insoluble particles at diameters below 2 nm. This demonstrates the importance of determining correct thermodynamics (like vapour pressures, activity coefficients and surface tensions) also for butanol/particle solutions. Nevertheless, the Kelvin diameter is larger than the activation diameter for soluble particles in all cases. The smaller the dry particle diameter, the bigger the contact angle can be before the Kelvin diameter drops below the activation diameter.

3.2. Detection efficiency of the UWCPC

Since the CPCB is based on four individual condensation particle counters we need to establish the detection efficiency of all individual devices. Detection efficiencies of the TSI-3010 and TSI-3025 have been reported as a result of extensive laboratory comparisons (Sem, 2002; Wiedensohler et al., 1997), as well as the working principles and detection efficiency of the water CPC, type TSI-3785 (Hering & Stoltzenburg, 2005; Hering et al., 2005; Petäjä et al., 2006). In this section, we complete the existing information by an experimental characterisation of the detection efficiency of the ultrafine water CPC (TSI-3786).

In a CPC the detection of submicrometer particles is based on their activation to optically visible droplets, typically several micrometers in diameter. In the TSI-3786 CPC an incoming aerosol sample is first conditioned to almost 100% relative humidity using a wetted wick on the outer wall of the saturator tube. The temperature of the conditioner wall is held constant (12 °C) in normal operating conditions. The actual growth of the sampled aerosol particles occurs in the growth tube, in which the wick is also kept wet but under a higher temperature of 75 °C. Close to the wick, the partial pressure of water vapour is close to equilibrium vapour pressure at the wick temperature. As the passing flow in the growth tube has a lower partial pressure of water vapour, diffusion of water vapour takes place towards the centreline of the sample flow. Since the molecular diffusivity of water vapour is higher than the thermal diffusivity of air, a region of supersaturated water vapour is created in the centre of the growth tube (Hering & Stoltzenburg, 2005). The key parameter determining the magnitude of supersaturation obtained within the growth tube is the temperature difference between the conditioner and the saturator: Higher temperature differences lead to higher supersaturations inside the growth tube. As a result, heterogeneous nucleation onto initially smaller particles is initiated and they are successfully counted with the optics of the instrument.

In this work, the detection efficiency of the Ultrafine Water CPC (TSI-3786) was determined using the calibration set-up as described by Petäjä et al. (2006). In this set-up monodisperse silver particles were generated by a combination

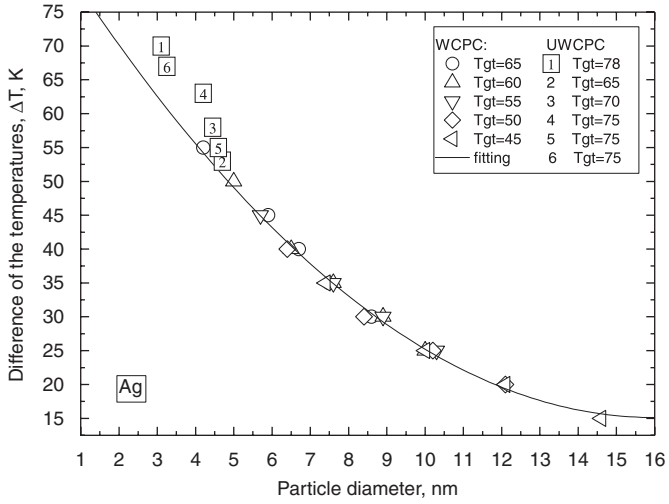

Fig. 5. Detection efficiency of the Water CPC (TSI- 3785) and Ultrafine Water CPC (TSI-3786) as a function of the temperature difference between saturator and growth tube for monodisperse silver particles. Increasing temperature differences lead to higher supersaturations so that heterogeneous nucleation of smaller particles becomes more probable.

of a furnace generator and a Vienna-type differential mobility particle sizer in a diameter range between 1 and 10 nm. During one set of experiments the saturator temperature was kept fixed at 12 °C with the growth tube temperatures being scanned from 65 to 75 °C. During other measurements the temperature of the growth tube was fixed to 75 °C and temperature of the saturator varied from 8 to 20 °C. In all of the detection efficiency curves the error bars represent the standard deviation of three independent measurements. The width of the transfer function of the nano-DMA, which becomes broader due to particle diffusion as smaller particle sizes are approached, is not considered in the determination of the CPC counting efficiency.

A conclusion of our calibrations was that the detection efficiency of the UWCPC TSI-3786 depends essentially on the saturator/growth tube temperature difference. Notably, the absolute temperatures had no noticeable effect on the CPC counting efficiency. Fig. 5 shows the CPC cut-off diameters as a function of temperature difference. It can be seen that the cut-off size increases with decreasing temperature difference as a result of elevated supersaturation inside the growth tube and subsequent activation of smaller particles. Therefore tuning of the TSI-3786 is possible so that cut-off sizes between 2 and 15 nm may be achieved (see Fig. 5).

When extrapolating the data in Fig. 5 beyond the range of temperature differences actually examined, it may be hypothesised that particles even smaller than 2 nm could be activated using this same technique. To make such measurements reality, larger temperature difference would need to be created, and transport losses in the instrument due to diffusion would need to be minimised. Fig. 5 suggests that using a temperature difference of 75 K, a cut-off size of 2 nm may be achieved. It is interesting to note that by tuning the temperature difference of the TSI-3786, the cut-off size can be reduced considerably compared to the nominal (manufacturer) temperature settings (see Fig. 6). In Fig. 6 the cut-off size of approximately 4.5 nm in default regime differs from the size 2.5 nm given in the manual (Liu, Odmondson, Sem, Quant, & Oberreit, 2005; TSI Inc., 2005). However, silver is not wettable by water as the particles used in the calibrations as described in the manual. We consider this difference as an indication for the material dependence of the cut-off size.

3.3. Effect of particle chemical composition on the detection efficiency

The purpose of the CPC battery is to distinguish aerosol particles based upon their activation properties in different vapour types. We now establish the performance of the CPCB for contrasting hydrophobic and hygroscopic test aerosols. As described above, both water CPCs were tuned such that the cut-off sizes of about 3 and 11 nm were matched within each CPC pair for insoluble silver particles. The counting efficiency curves of the four individual instruments that form the CPCB are summarised in Fig. 7. The temperature settings in this optimum state were: UWCPC, saturator: 8 °C,

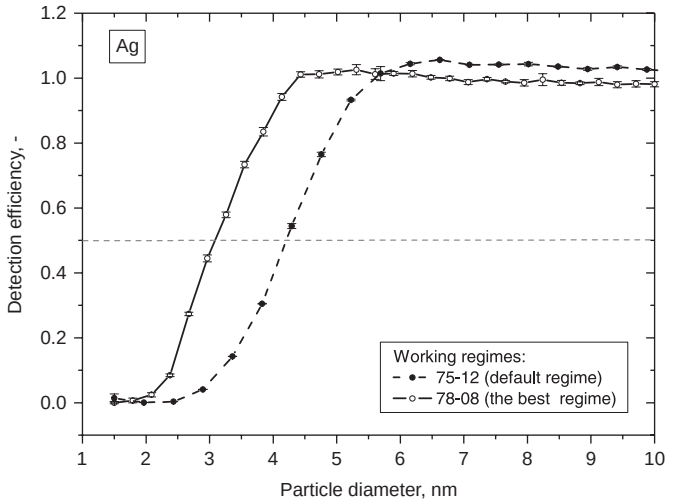

Fig. 6. Detection efficiency of the Ultrafine Water CPC (TSI-3786) for the manufacturer's default settings as well as for the optimal settings with respect to lower detection limit.

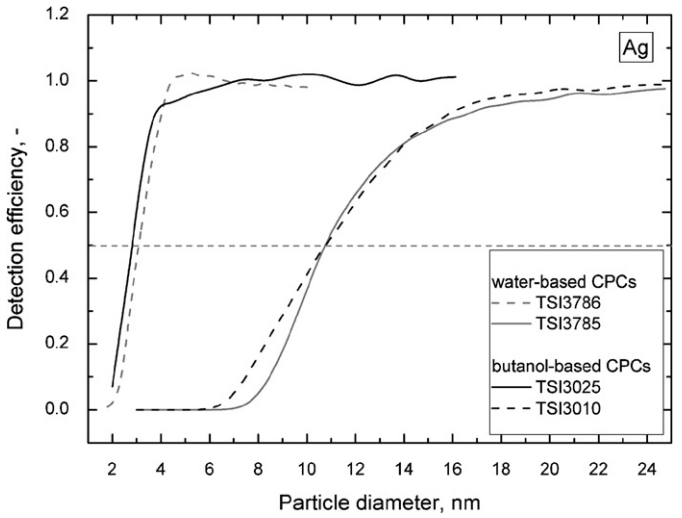

Fig. 7. Detection efficiency curves for silver particles of the four individual CPCs as operated in the CPC battery.

growth tube: 78 °C; WCPC, saturator: 30 °C, growth tube: 55 °C. The two butanol CPCs were operated under their standard manufacturer settings: TSI-3025, saturator: 37 °C, condenser 10 °C, and the TSI-3010 at $\Delta T = 17$ K.

While an increased activation efficiency of hygroscopic particles in the WCPC (TSI-3785) has been reported elsewhere (Hering et al., 2005; Petäjä et al., 2006), no quantitative corresponding information has been available for the UWCPC (TSI-3786). Like in previous studies, silver particles were used as an insoluble particle type, and sodium chloride and ammonium sulphate as water soluble particle types. As can be seen from our calibrations in Fig. 8, the detection efficiency decreases as a function of size and is, as expected, dependent on chemical particle composition. While the cut-off diameter for silver particles is about 3 nm, it decreases remarkably for ammonium sulphate (2.3 nm) and even further for NaCl (1.8 nm). These cut-off diameters show an overall agreement with our theoretical calculations (Fig. 4a).

Our observed dependency of the lower cut-off size on particle chemical composition parallels some of the results obtained by Hering et al. (2005), who compared a TSI-3785 water CPC to a TSI-3025 butanol UCPC. Particles

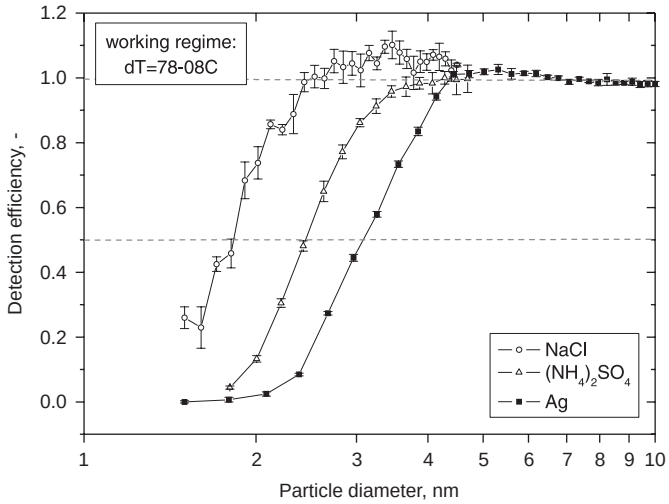

Fig. 8. Detection efficiency of the Ultrafine Water CPC (TSI-3786) for particles of different chemical composition.

composed of water soluble inorganic salts (ammonium sulphate, ammonium nitrate, sodium chloride) were detected more efficiently, with cut-off size of 4.5, 4.7 and 3.6 nm, respectively. For pure dioctyl sebacate (DOS) vapour the cut-off size was as large as 30 nm, but as soon as this was mixed with just 4 ppt of sodium chloride the cut-off diameter decreased to 13 nm. In conclusion, the laboratory calibrations strongly support the feasibility of the CPC battery as a classification method that is sensitive to the chemical composition of small particles.

3.4. The use of heterogeneous nucleation theorem and the number of molecules at aerosol particle surface

The number of molecules Δn_{het} in the critical cluster (see Appendix) can be obtained by the following iterative procedure which consists of two steps: (a) the first step, in which no prior information about the radius of the critical cluster is available for the calculation of the factors f_g and f_n (see Appendix), uses as starting point the Kelvin equation (see Appendix Eq. (A.1)), and (b) the second step, in which a convergent solution is obtained. The first step allows us to calculate the initial values for the number of molecules from Eq. (A.11). These numbers represent the input for the second step, where Eq. (A.11) is solved by iterations and the radius is calculated using the number of molecules in the critical cluster. The procedure converges after few iteration steps.

First we estimated the number of molecules in the cluster for water nucleating on silver particles. The temperature difference was 70 K (saturator: 8 °C, growth tube: 78 °C). In calculations the saturation ratio was set to 2.3 and the temperature at 310 K. The cosine of the contact angle was estimated to be 0.14 (see e.g., Wagner et al., 2003). The number of the molecules decreases from 16 to 5 as diameter of seed particle is increasing from 2.8 to 5 nm. For the studied temperature difference, the number of molecules in the cluster doesn't vary considerably, ranging from 4 to 12. As a sensitivity test we decreased the value of the contact angle, and thus increasing the cosine up to 1. As a result the number of molecules decreases considerably down to 3–6.

Secondly, a similar procedure was used for determining the number of molecules of butanol in critical clusters on silver seed particles. In this case the saturation ratio and temperature were set to 2.0 and 290 K, respectively, and the calculated cosine of the contact angle was $m = 0.95$. The critical cluster contains only a few (3–6) butanol molecules.

3.5. Ambient aerosol study

To demonstrate the feasibility of field measurements using the CPCB, atmospheric observations were conducted during April and May 2005 at the Station for Measuring Forest Ecosystem–Atmosphere Relation (SMEAR-II) in Hyytiälä, Southern Finland (see e.g. Kulmala, Hämeri, et al., 2001). As for laboratory aerosols, the CPCB was expected to reveal any existing affinity of environmental particles towards water or butanol. During the experiment, all four CPCs were operated in their CPCB reference state as described in Section 3.3, and counted total ambient particle concentrations at a frequency of 1 Hz.

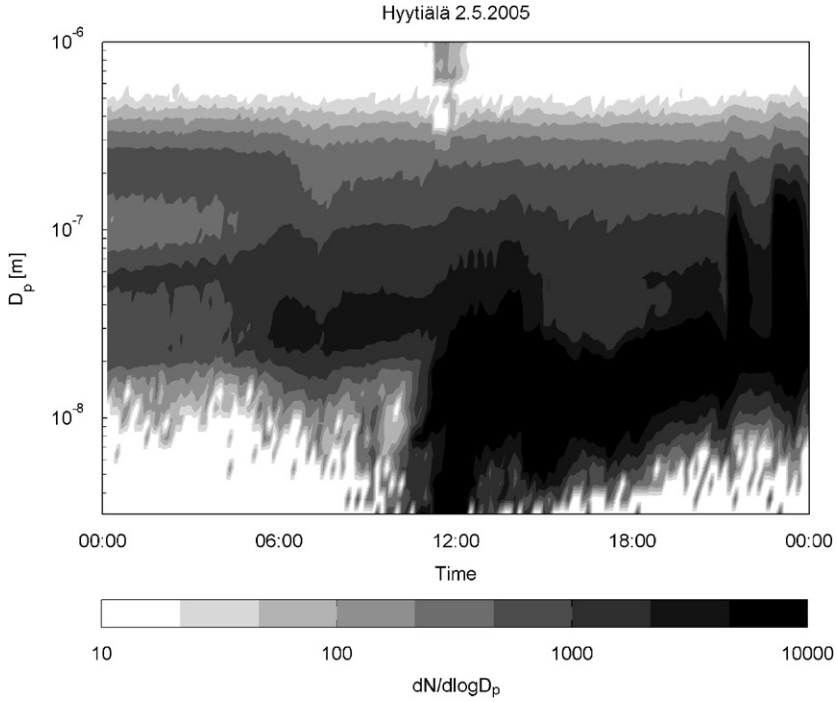

Fig. 9. The diurnal evolution of the particle size distribution measured with a DMPS system during a nucleation event in Hyytiälä, Finland, on May 2, 2005.

The CPCB measurements were complemented by particle size distribution measurements using a dual DMPS (differential mobility particle sizer) system covering a size range of 3–900 nm, and a APS (aerodynamical particle sizer TSI-3320), covering particle sizes between 0.7 and 20 μm. In addition, air ions were detected using a BSMA (The Balanced Scanning Mobility Analyzer, AIREL, Ltd, Tartu, Estonia) and a AIS (Air Ion Spectrometer, AIREL, Ltd, Tartu, Estonia) (Laakso et al., 2004) (data not shown here).

During the measurement period, several new particle formation (nucleation) events occurred in tropospheric air at Hyytiälä. One of the particle formation events, on May 2, 2005 was chosen for closer inspection. Fig. 9 shows the diurnal cycle of the particle size distribution. The simultaneously measured variation of the particle number concentrations measured by the four individual CPCs of the CPCB are shown in Fig. 10.

The nucleation event started around 9:30 a.m. local time, when the total particle number concentrations measured by the CPCB increased by more than one order of magnitude. The increase in the concentrations measured by the WCPC and the UWCPC was simultaneous within 15 min. Most notably, the number concentration difference between the UWCPC and UCPC increased at the same time. A maximum difference of 6000 cm^{-3} could be seen at 11:30 between the CPC pair with nominal cut-off size 3 nm, and 1500 cm^{-3} at 12:30 for the CPC pair with cut-off size 11 nm. After midday the concentration difference between WCPC and CPC decreased again. Our basic conclusion is that the particles formed during the observed nucleation events tended to be hydrophilic both, at 3 and 11 nm. The results indicate that a relevant fraction of soluble material is present in nucleation mode particles. This could point to the involvement of sulphuric acid during the early particle formation and growth process as opposed to low volatility organic compounds.

After 21:00, particle concentrations increased not as a result of new particle formation, but due to advection of pollution, as can be seen also in trace gas (e.g. NO_x) concentrations (data not shown here). During this pollution episode, the total particle concentrations attain similar as during the particle formation event, but this time the readings of the water CPCs do not exceed the readings of the butanol CPCs. This demonstrates that the differential signal obtained from the two CPC pairs within the CPC battery is not a function of total particle concentration, but rather particle chemical composition, so that the working principle of the CPC battery is valid under atmospheric applications.

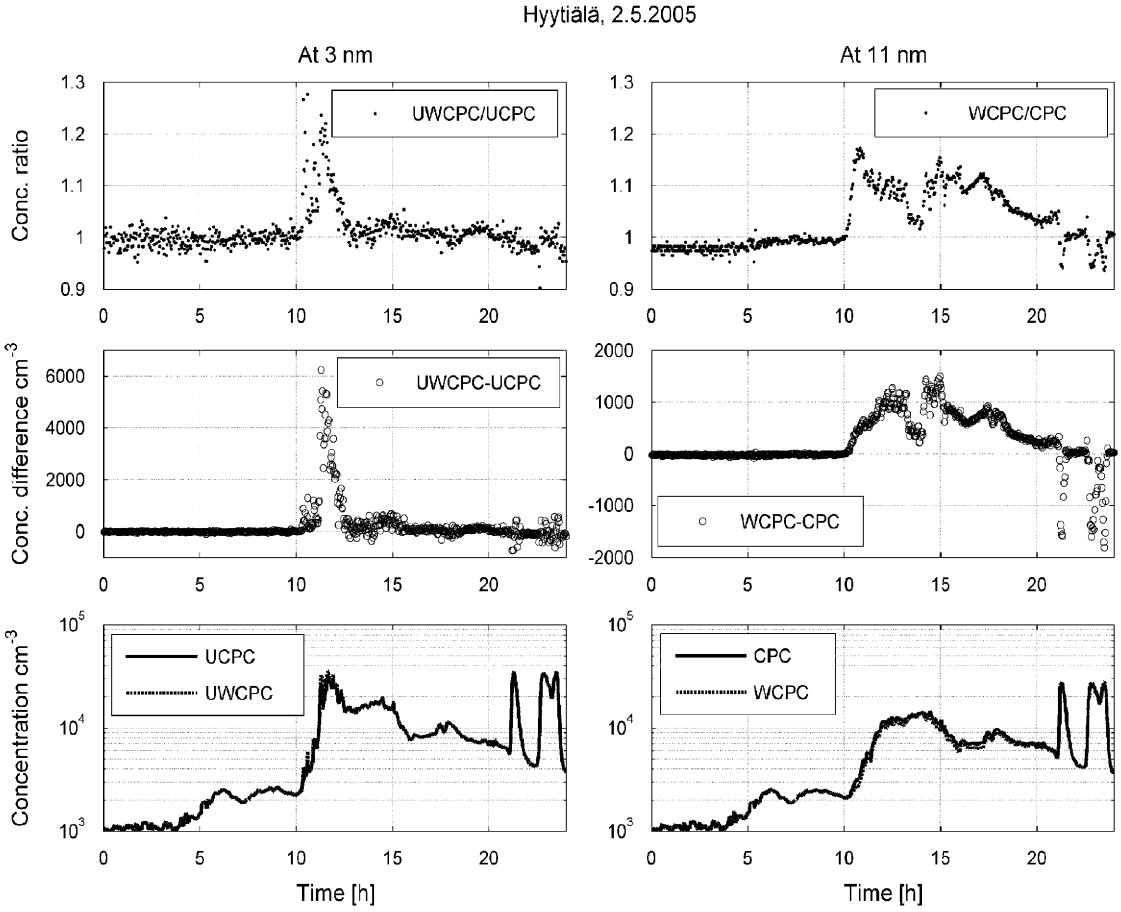

Fig. 10. The daily variation of the total number concentration measured by CPCB. The left column refers to ultrafine CPCs TSI-3786 (UWCPC) and TSI-3025 (UCPC), and the right column to TSI-3785 (WCPC) and TSI-3010 (CPC). The bottom figures present measured total number concentrations; middle—the absolute difference of the total concentrations; and top-relative differences between the water- and butanol-based CPCs.

To estimate the cut-off sizes of the water CPCs in the observed ambient conditions, we simulated a nucleation mode with the geometrical mean diameter growing from 1 to 30 nm in an environment with a background aerosol (diameter larger than 30 nm) concentration of 2000 cm^{-3}. The nucleation mode concentration was set to 8000 cm^{-3} and the geometric standard deviation varied from 1.3 to 1.5. The concentrations and modal parameters were chosen to correspond to the experimental observations on May 2, 2005. The simulated nucleation mode was first weighted with the detection efficiency curves of the CPCs (cut-off sizes 3 and 11 nm, see Fig. 7) to investigate the individual differences between the water and butanol CPCs assuming uniform insoluble Ag particles. According to the calculations, the maximum concentration difference resulting from the different shape of the detection efficiency curves was in the order of 15% for UWCPC and UCPC and approximately −9% for WCPC and CPC. However, the observed difference between the UWCPC and UCPCs is almost 30%; in the case of WCPC and CPC the corresponding difference is 17%. To obtain the differences observed with the ambient (more water soluble) aerosol, we had to shift the cut-off sizes of the water CPCs approximately 0.5 nm (UWCPC) and 1.5 nm (WCPC). We can therefore estimate the ambient cut-off size of the UWCPC to be around 2.5 nm and for the WCPC around 9.5 nm.

Also, we made simulations using the measurement data from CPCB and DMPS systems. We interpolated counting efficiencies (Fig. 7) of CPC and WCPC to the DMPS channels. In addition, for water CPC we generated a series of counting efficiency curves by shifting the curve by increasing increments to the left. Consistently with the theoretical study described above, we found that the cut-off size of the WCPC during the particle formation was shifted approximately to 9.5 nm.

4. Conclusions

In this paper we present the principle of the condensation particle counter battery (CPCB). The CPCB consists of two water based and two butanol based CPCs (namely TSI-3785, TSI-3786, TSI-3010 and TSI-3025). The rationale for the design of the CPCB is based on its ability to distinguish aerosol particles of different chemical composition through their activation properties in different vapours. For particles of a given composition, the activation probability was shown to depend on the supersaturations achieved in the CPC, which were in turn almost exclusive functions of the temperature difference between saturator and condenser. Theoretical calculations and laboratory experiments demonstrated that soluble particles will be detected down to lower cut-off sizes in the water-based CPCs. In the case of insoluble particles the surface properties, particularly the contact angle, determines how the particles will activate.

Theoretical calculations showed that homogeneous nucleation inside the CPCs can be avoided as long as the activation diameters are smaller than the Kelvin diameters, which proved to be the case for soluble and totally wettable particles. When the diameter is below 2 nm, the ratios of different activation diameters are changing. However, all those being already below Kelvin diameter stay there. We can even say that the heterogeneous nucleation is more effective in the case of small particles as compared to homogeneous nucleation.

The use of heterogeneous nucleation theorem gives the opportunity to find out the number of molecules in the critical cluster. This will give us further insight on surface properties of nanoparticles. However, more laboratory investigation is needed before we can determine surface properties in situ.

Careful calibrations of the cut-off diameters as a function of temperature difference between saturator and growth tube were accomplished for the water-based CPCs in order to match the cut-off sizes given by the butanol-based CPCs. However, we have also performed comparative test in the laboratory. The optimal temperature difference for TSI3786 was found to be 70 K. The dependence of cut-off diameter on particle composition has been determined, and the results have been found to be qualitatively consistent with theoretical ones and quantitatively with earlier experiments.

Atmospheric field measurements performed at a rural background site in Finland (Hyytiälä) demonstrated the applicability of the CPCB to atmospheric nanoparticles. The CPCB data indicate that freshly formed particles at 3 and 11 nm contain water soluble material.

In the future the CPCB will require further characterisation in the laboratory and will be deployed in different atmospheric environments. There is a hope that the CPCB will help elucidate the chemical composition of newly formed nanoparticles and, therefore, the selection of gas phase precursors involved in the formation of new atmospheric nuclei.

Appendix A

A.1. Use of heterogeneous nucleation theorem at constant saturation ratio

According to the nucleation theorem the slope of the nucleation rate as a function of the concentration of the nucleating vapour determines the number of molecules in the critical cluster (Kashchiev, 1982). The nucleation theorem is valid also for heterogeneous nucleation (Vehkamäki, Lauri, Määttänen, & Kulmala, 2005; Kashchiev, 2000). In the case of heterogeneous nucleation the number of molecules in the critical cluster depends not only on the saturation ratio, but also on the contact angle and the ratio of radii of the seed particle and the critical cluster (Määttänen et al., 2005; Kulmala, Lauri, et al., 2001; Kulmala, Hämeri, et al., 2001; Vehkamäki et al., 2005). In CPC studies, the nucleation probability is given primarily as a function of dry particle size, and not as a function of the vapour concentration. Therefore, we need to modify the heterogeneous nucleation theorem in the following way.

The theoretical radius of the critical cluster r^* can be calculated using the Kelvin equation

$$r^* = \frac{2\sigma v_i}{kT \ln S}, \tag{A.1}$$

where S is the experimental saturation ratio. The ratio of dry particle size and the size of the critical cluster is denoted by X

$$X \equiv \frac{R_{\mathrm{dry}}}{r^*} = \frac{R_{\mathrm{dry}} kT \ln S}{2 v_i \sigma}. \tag{A.2}$$

In classical heterogeneous nucleation the formation energy of the critical heterogeneous nuclei is related to the formation energy of homogeneous nuclei

$$\Delta G_{\text{het}} = f_g(m, X)\Delta G_{\text{hom}}, \tag{A.3}$$

where

$$f_g = \frac{1}{2}\left[1 + \left(\frac{1 - Xm}{g}\right)^3 - X^3\left(2 - 3\left(\frac{X - m}{g}\right) + \left(\frac{X - m}{g}\right)^3\right) + 3X^2\left(\frac{X - m}{g} - 1\right)\right]$$

with

$$g = \sqrt{1 + X^2 - 2Xm}$$

is a geometric factor (see e.g. Lazaridis et al., 1992) and $m = \cos\theta$, where θ is the contact angle. Also the number of molecules in the critical heterogeneous cluster Δn_{het} is connected to the homogeneous case

$$\Delta n_{\text{het}} = f_n(m, X)\Delta n_{\text{hom}}, \tag{A.4}$$

where

$$f_n = \frac{1}{4}\left[2 + 3\left(\frac{1 - Xm}{g}\right) - \left(\frac{1 - Xm}{g}\right)^3 - X^3\left(2 - 3\left(\frac{X - m}{g}\right) + \left(\frac{X - m}{g}\right)^3\right)\right]$$

is another geometric factor (Määttänen et al., 2005).

The geometrical factors satisfy a relation

$$-\frac{X}{2}\left(\frac{\partial f_g}{\partial X}\right)_m = f_n - f_g. \tag{A.5}$$

The derivative of $-\Delta G_{\text{het}}/(kT)$ with respect to the dry particle radius is

$$\begin{aligned}\frac{\partial \frac{-\Delta G_{\text{het}}}{kT}}{\partial R_{\text{dry}}} &= \frac{-\partial f_g}{\partial R_{\text{dry}}}\frac{\Delta G_{\text{hom}}}{kT} = \frac{-\partial f_g}{\partial X}\frac{\partial X}{\partial R_{\text{dry}}}\frac{\Delta G_{\text{hom}}}{kT} = \frac{-\partial f_g}{\partial X}\frac{kT\ln S}{2v_i\sigma}\frac{4\pi r^{*2}\sigma}{3kT}\frac{1}{kT}\\ &= \frac{-\partial f_g}{\partial X}\frac{1}{r^*}\frac{\ln S}{2}\frac{4\pi r^{*3}}{3kTv_i} = \frac{-X}{2}\frac{\partial f_g}{\partial X}\frac{\ln S}{R_{\text{dry}}}\Delta n_{\text{hom}} = (f_n - f_g)\frac{\ln S}{R_{\text{dry}}}\Delta n_{\text{hom}}\\ &= f_n\left(1 - \frac{f_g}{f_n}\right)\frac{\ln S}{R_{\text{dry}}}\Delta n_{\text{hom}} = \left(1 - \frac{f_g}{f_n}\right)\frac{\ln S}{R_{\text{dry}}}\Delta n_{\text{het}},\end{aligned} \tag{A.6}$$

where we have used classical expressions

$$\Delta G_{\text{hom}} = \frac{4\pi r^{*2}\sigma}{3kT} \tag{A.7}$$

and

$$\Delta n_{\text{hom}} = \frac{4\pi r^{*3}}{3kTv_i}. \tag{A.8}$$

The nucleation rate J_{het} is given by

$$J_{\text{het}} = K\exp\left(\frac{-\Delta G_{\text{het}}}{kT}\right), \tag{A.9}$$

where K is a kinetic pre-factor which depends only weakly on the dry particle radius.

The probability that heterogeneous nucleation occurs in a constant time period t is related to the nucleation rate through

$$P = 1 - \exp(-J_{\text{het}} t) \tag{A.10}$$

and thus

$$\left(\frac{\partial \ln\left(\ln \frac{1}{1-P}\right)}{\partial R_{\text{dry}}}\right) = \left(\frac{\partial \ln J_{\text{het}}}{\partial R_{\text{dry}}}\right) = \left(\frac{\partial \frac{-\Delta G_{\text{het}}}{kT}}{\partial R_{\text{dry}}}\right) + \left(\frac{\partial \ln K}{\partial R_{\text{dry}}}\right) \approx \left(1 - \frac{f_g}{f_n}\right) \frac{\ln S}{R_{\text{dry}}} \Delta n_{\text{het}}. \tag{A.11}$$

Using CPC detection efficiency measurements together with Eq. (A.11) we can obtain information about the number of molecules in the critical clusters forming on aerosol particles inside the CPC.

References

Birmili, W., Berresheim, H., Plass-Dülmer, C., Elste, T., Gilge, S., Wiedensohler, A. et al. (2003). The Hohenpeissenberg aerosol formation experiment (HAFEX): a long-term study including size-resolved aerosol, H_2SO_4, OH, and monoterpenes measurements. *Atmospheric Chemistry and Physics*, *3*, 361–376.

Biswas, S., Fine, P. M., Geller, M. D., Hering, S. V., & Sioutas, C. (2005). Performance evaluation of a recently developed water-based condensation particle counter. *Aerosol Science and Technology*, *39*, 419–427.

Brock, C. A., Schröder, F., Kärcher, B., Petzold, A., Busen, R., & Fiebig, M. (2000). Ultrafine particle size distributions measured in aircraft exhaust plumes. *Journal of Geophysical Research*, *105*, 26555–26568.

Cabada, J. C., Khlystov, A., Wittig, A. E., Pilinis, C., & Pandis, S. N. (2004). Light scattering by fine particles during the Pittsburgh air quality study: Measurements and modelling. *Journal of Geophysical Research*, *109*, D16S03.

Donaldson, K., Li, X., & MacNee, W. (1998). Ultra-fine (nanometer) particle-mediated lung injury. *Journal of Aerosol Science*, *29*, 553–560.

Hämeri, K., Laaksonen, A., Väkevä, M., & Suni, T. (2001). Hygroscopic growth of ultrafine sodium chloride particles. *Journal of Geophysical Research*, *106*, 20749–20757.

Hämeri, K., Koponen, I. K., Aalto, P. P., & Kulmala, M. (2002). The particle detection efficiency of the TSI-3007 condensation particle counter. *Journal of Aerosol Science*, *33*, 1463–1469.

Hämeri, K., Väkevä, M., Hansson, H.-C., & Laaksonen, A. (2000). Hygroscopic growth of ultrafine ammonium sulphate aerosol measured using an ultrafine tandem differential mobility analyser. *Journal of Geophysical Research*, *105*, 22231–22242.

Hering, S. V., & Stoltzenburg, M. R. (2005). A method for particle size amplification by water condensation in a laminar, thermally diffusive flow. *Aerosol Science and Technology*, *39*, 428–436.

Hering, S. V., Stoltzenburg, M. R., Quant, F. R., Oberreit, D. R., & Keady, P. B. (2005). A laminar-flow, water-based condensation particle counter (WCPC). *Aerosol Science and Technology*, *39*, 659–672.

Kashchiev, D. (1982). On the relation between nucleation work, nucleus size, and nucleation rate. *Journal of Chemical Physics*, *76*, 5098–5102.

Kashchiev, D. (2000). *Nucleation: Basic theory with applications*. Oxford: Butterworth-Heinemann.

Kulmala, M. (2003). How particles nucleate and grow. *Science*, *302*, 1000–1001.

Kulmala, M., Hämeri, K., Aalto, P. P., Mäkelä, J. M., Pirjola, L., Nilsson, E. D. et al. (2001). Overview of the international project on biogenic aerosol formation in the boreal forest (BIOFOR). *Tellus*, *53B*, 324–343.

Kulmala, M., Kerminen, V.-M., Anttila, T., Laaksonen, A., & O'Dowd, C. D. (2004). Organic aerosol formation via sulphate cluster activation. *Journal of Geophysical Research*, *109*(D4), 4205.

Kulmala, M., Lauri, A., Vehkamäki, H., Laaksonen, A., Petersen, D., & Wagner, P. E. (2001). Strange predictions by binary heterogeneous nucleation theory compared with a quantitative experiment. *Journal of Physical Chemistry B*, *105*, 11800–11808.

Kulmala, M., Lehtinen, K. E. J., Laakso, L., Mordas, G., & Hämeri, K. (2005). On the existence of neutral atmospheric clusters. *Boreal Environment Research*, *10*, 79–87.

Kulmala, M., Vehkamäki, H., Petäjä, T., Dal Maso, M., Lauri, A., Kerminen, V.-M. et al. (2004). Formation and growth rates of ultrafine atmospheric particles: A review of observations. *Journal of Aerosol Science*, *35*, 143–176.

Laakso, L., Anttila, T., Lehtinen, K. E. J., Aalto, P. P., Kulmala, M., Hõrrak, U. et al. (2004). Kinetic nucleation and ions in boreal particle formation events. *Atmospheric Chemistry and Physics*, *4*, 2353–2366.

Lazaridis, M., Kulmala, M., & Gorbunov, B. Z. (1992). Binary heterogneous nulceation at a non-uniform surface. *Journal of Aerosol Science*, *23*, 457–466.

Liu, W., Odmondson, B. L., Sem, G. J., Quant, F. R., & Oberreit, D. (2005). *Water-based condensation counters for environmental monitoring of ultrafine particles*. An international speciality conference, Atlanta, Georgia, USA, February 2005.

Lohmann, U., & Feichter, J. (2005). Global indirect aerosol effects: A review. *Atmospheric Chemistry and Physics*, *5*, 715–737.

Määttänen, A., Vehkamäki, H., Lauri, A., Merikallio, S., Kauhanen, J., Savijärvi, H. et al. (2005). Nucleation studies in the Martian atmosphere. *Journal of Geophysical Research*, *110*(E2), E02002.

McMurry, P. H. (2000). The history of CPCs. *Aerosol Science and Technology*, *33*, 297–322.

O'Dowd, C. D., Aalto, P., Hameri, K., Kulmala, M., & Hoffmann, T. (2002). Aerosol formation: Atmospheric particles from organic vapours. *Nature*, *6880*, 497.

Petäjä, T., Mordas, G., Manninen, H., Aalto, P. P., Hämeri, K., & Kulmala, M. (2006). Detection efficiency of a water-based TSI condensation particle counter 3785. *Aerosol Science and Technology*, *40*, 1090–1097.

Ramanathan, V., Crutzen, P. J., Kiehl, J. T., & Rosenfeld, D. (2001). Aerosol, climate and the hydrological cycle. *Science*, *294*, 2119–2124.

Scheibel, H. G., & Porstendörfer, J. (1983). Generation of monodisperse AG- and NaCl-aerosols with particle diameters between 2 and 300 nm. *Journal of Aerosol Science*, *14*, 113–126.

Seinfeld, J. H., & Pandis, S. N. (1998). *Atmospheric chemistry and physics, From air pollution to climate change*. New York: Wiley.

Sekiguchi, M., Nakajima, T., Suzuki, K., Kawamoto, K., Higurashi, A., Rosenfeld, D. et al. (2003). A study of the direct and indirect effects of aerosols using global satellite data sets of aerosol and cloud parameters. *Journal of Geophysical Research*, *108*(D22), 4699.

Sem, G. J. (2002). Design and performance characteristics of three continuous-flow condensation particle counters: a summary. *Atmospheric Research*, *62*, 267–294.

Sgro, L. A., & Fernández de la Mora, J. (2004). A simple turbulent mixing CNC for charged particle detection down to 1.2 nm. *Aerosol Science and Technology*, *38*, 1–11.

Smith, J. N., Moore, K. F., Eisele, F. L., Voisin, D., Ghimire, A. K., Sakurai, H. et al. (2005). Chemical composition of atmospheric nanoparticles during nucleation events in Atlanta. *Journal of Geophysical Research*, *110*, D22S03.

Stieb, D. M., Judek, S., & Burnett, R. T. (2002). Meta-analysis of time-series studies of air pollution and mortality: Effects of gases and particles and their influence of cause of death, age and season. *Journal of the Air and Waste Management Association*, *52*, 470–484.

Stoltzenburg, M. R., & McMurry, P. H. (1991). An ultrafine aerosol condensation nucleus counter. *Aerosol Science and Technology*, *14*, 48–65.

TSI Inc., (2005). *Model 3786 Ultrafine water-based condensation particle counter*: *Operation and service manual*, P/N 1930072, Revision A, TSI Inc., January 2005.

Väkevä, M., Kulmala, M., Stratmann, F., & Hämeri, K. (2002). Field measurements of hygroscopic properties and state of mixing of nucleation mode particles. *Atmospheric Chemistry and Physics*, *2*, 55–66.

Vehkamäki, H., Lauri, A., Määttänen, A., Kulmala, M. (2005). Nucleation theorems for heterogeneous nucleation. *Proceedings of European Nucleation Conference* 2005, 28 August–2 September, Ghent, Belgium. p. 34.

Wagner, P. E., Kaller, D., Virtala, A., Lauri, A., Kulmala, M., & Laaksonen, A. (2003). Nucleation probability in binary heterogeneous nucleation of water-n-propanol vapour mixtures on insoluble and soluble nanoparticles. *Physical Review E*, *67*, Art.No. 021605.

Weber, R. J., McMurry, P. H., Mauldin, R. L., Tanner, D. J., Eisele, F. L., Clarke, A. D. et al. (1999). New particle formation in the remote troposphere: A comparison of observations at various sites. *Geophysical Research Letters*, *26*(3), 307–310.

Wehner, B., Petäjä, T., Boy, M., Engler, C., Birmili, W., Tuch, T. et al. (2005). The contribution of sulfuric acid and non-volatile compounds on the growth of freshly formed atmospheric aerosols. *Geophysical Research Letters*, *32*, L17810.

Wiedensohler, A., Orsini, D., Covert, D. S., Coffmann, D., Cantrell, W., Havlicek, M. et al. (1997). Intercomparison study of the size-dependent counting efficiency of 26 condensation particle counters. *Aerosol Science and Technology*, *27*, 224–242.